Chelate stabilized metal oxides for visible light photocatalyzed water oxidations

Dominic Walsh[a]*, Noelia M. Sanchez-Ballester[b], Katsuhiko Ariga[b], Akihiro Tanaka[c] and Mark Weller[a]*

Visible light driven photocatalytic water oxidations were undertaken that compared lactate stabilized molecular and nanoparticle cobalt complexes and calcium manganese oxides as simple mimics of the PSII $CaMn_4O_5$ catalyst. Analysis showed chelated cobalt oxides formed as <5nm particles whilst Ca-Mn and Mn oxides were composed of nanoparticles organized into ~150nm spherules. O_2 yield, turnover frequency and quantum yields were determined for the chelated materials and compared to sintered $CaMn_3O_6$ and Co_3O_4 counterparts. Results show two distinct stages of O_2 generation took place with the chelated calcium manganese oxides, a Ca:Mn molar ratio of 1:3 gave highest O_2 yield in the initial stage. Significantly, O_2 generation at extended reaction time re-occurred without addition of fresh reagents and was determined to be promoted by in-situ coating of the lactate metal oxide particles with cobalt captured from the decomposed pentaminecobalt(III) chloride electron acceptor. Time course TEM, XPS and EDX analysis indicated the secondary catalyst accumulated cobalt mainly as Co_3O_4. These nano-micro particles are readily reused and produced a superior O_2 output of 85% maximum theoretical yield. Chelated cobalt catalysts resulted in TOF and O_2 yield superior to a laser ablated counterpart, whereas calcium manganese oxide lactates promoted generation of effective recyclable water oxidation catalysts which also minimized toxicity and waste for the photocatalytic system

Introduction

Solar driven approaches to energy production are becoming increasingly important areas for research and application. Whilst photovoltaic solar cells have been developed, refined and reached the stage of widespread implementation, artificial photosynthesis represents a new avenue for applied research. Sustainable energy production based on the photosynthetic process is an appealing approach for the generation of liquid fuels, however major improvements in terms of efficiency and costs are still required to bring this technology towards commercialisation.

The light driven oxidation of water is a successive four electron redox process and takes place in nature in the chloroplast photosystem II (PSII) which itself contains the oxygen evolving centre (OEC). This consists of a calcium-manganese oxide cluster catalyst, $CaMn_4O_5$, held in place within a protein support structure with several of the surrounding proteins terminated by carboxylated amino acids.[1-3] Significantly, as far as is known the OEC catalyst cluster composition is ubiquitous amongst light driven natural photosynthesis, though the surrounding protein structure varies to some degree between organisms. The calcium ion is known to be an essential co-factor, central to its role is that the ion has a fixed +2 charge. Ca^{2+} is believed to facilitate the formation of more highly oxidized Mn ions and effects the redox properties of the cluster as well has having some basic structural role.[4-8] It has also been proposed that a Mn^{3+}-(O^{2-})-Ca^{2+} intermediate exists in the PSII S_4 O_2 release state.[3]

An ultimate aim in artificial photosynthesis is a cell in which the protons and electrons generated can be used for hydrogen production at an electrode or for reduction of CO_2 into short chain hydrocarbons such as methane and methanol.[9, 10] This is analogous to natural PSII and PSI systems, and similarly the artificial systems envisaged are driven by visible light. Since the first reports by Harriman,[11, 12] many studies of artificial photosynthesis systems have been undertaken. Common to most of these are the requirement of a light absorbing sensitizer dye and a sacrificial acceptor to capture electrons promoted to accessible higher energy levels of the dye. A catalyst then forms a powerful oxidizing agent upon electron donation back to the dye and water is oxidized into gaseous O_2, protons and electrons at the catalyst surface. Persulphate has traditionally been used most frequently as an electron acceptor and this practice persists. However the powerful sulphate anion radical is generated in photochemical oxidations making its use somewhat undesirable, particularly with reagent mixtures more rich in organics. Besides persulphate, pentaminecobalt(III)chloride is now a commonly employed sacrificial oxidant and was used in this work. Whilst the cobalt complex has several benefits in comparison, the results shown here appear to have some general implications for its usage.

Previously, ruthenium or iridium metal oxides or complexes have been successfully employed as the catalyst,[13-15] and recently cobalt oxides or ligated cobalt complexes have been shown to be effective agents for the water oxidation reaction.[16-18] The photocatalytic reactions are typically conducted in a degassed aqueous buffer solution.

$$2H_2O + 4h\nu \rightarrow O_2\uparrow + 4H^+ \text{ (to buffer)} + 4e^- \text{ (to electron acceptor)}$$

Whilst significant advances have been made in terms of catalyst and/ or co-catalyst light sensitizer efficiency, the Turn Over Frequencies (TOF's) lie several orders of magnitude less than that of natural photosynthesis, which has reported TOF's ranging from ~25-80.[3, 19] Natural photosynthesis has evolved over a period exceeding 2 billion years and includes a protein support and repair system which cannot be replicated artificially to any extent at present. This means that current artificial systems typically have reaction lifetimes around 30-60 min due to decomposition of the components, as well as using high cost and/or toxic catalysts and light sensitizers in order to obtain reasonable TOF's.

Here we used lactic acid as low cost and eco-friendly chelating agent. This can coordinate to metal ions through an oxygen atom of the carboxylate group and the oxygen of the adjacent hydroxyl group. Lactate binding inhibited bulk precipitation and further crystal growth and stable fully dispersible cobalt catalysts were synthesized, in the form of a molecular or nanoparticulate Co^{2+} lactate hydroxide depending on lactate level. Also a range of chelate stabilized calcium manganese oxides were prepared. All metal oxide particles were prepared without recourse to high temperature methods. The bimetallic CaMn oxide materials represent a possible primitive form of the PSII catalyst in its early evolution stages and as such their study may help to elucidate how these bimetallic oxides with bound organics may have functioned and developed.[20] The presence of the organic stabilizing agent also allows future direct and facile linking of catalyst to supports and/or photosensitizer and hence the prospect of improved efficiency.

Previously calcium manganese oxides have been prepared as crystalline or amorphous phases by high temperature heating and tested for water oxidation.[7, 21, 22] It has been found that these sintered materials are effective catalysts though often less efficient compared to rare earth or cobalt oxide, however Ca-Mn oxides have the appealing advantage of being abundant and low toxicity biomimics.[8]

Significantly, the bimetallic oxides prepared here exclusively gave a successive stage when the catalyst had re-organized in-situ, re-accumulated sufficient charge and a secondary active water oxidation state reached, this was examined by a time course study. To our knowledge such a secondary phase of O_2 generation at such extended reaction time without addition of fresh reagents has not previously been reported. Comparison to metal oxide catalysts prepared via high temperature heating routes was made. O_2 release and pH changes for these reactions were monitored in-situ. We demonstrate that chelation reduced waste and produced prolonged reaction lifetimes.

Results and discussion

Characterization of catalyst materials

The preparations resulted in a range of lactate stabilized metal oxide solids that dispersed up into water to give coloured suspensions. Manganese based preparations rapidly converted into loosely aggregated flocs that partially settled out on standing. Upon light shaking these flocs fully re-dispersed back into solution. However Co-lac samples formed a ruby red or brown/red nanosuspension at Co:lactate of 1:2 and 1:1 molar ratios respectively. These suspensions were stable for 3 days before onset of formation of a black cobalt oxide/hydroxide precipitate (ESI† Fig. S1a).

Infra-red spectroscopy measurements of the chelated samples showed a marked red shift of the lactic acid carboxyl band. For calcium-manganese oxides a shift from 1730cm^{-1} to give a ν_{as} band at 1555cm^{-1} for the lactate $-CO_2M$ was obtained.[23] A CO_2M stretch was also introduced at 1400cm^{-1}, the absorbance of this band increased relative to the ν_{as} band with the Ca^{2+} presence, suggesting both $-CO_2Ca$ and $-CO_2Mn$ chelation was present. The bands between 1130-1000cm^{-1} correspond to OH bends and C-O stretches (Fig. 1a-f).

Quantitative spot EDX analysis of the prepared oxide particles was conducted which showed mean Ca:Mn molar ratios of 1:4.12 and 1:3.08 for $CaMn_4Ox$-lactate and $CaMn_3Ox$-lactate respectively with high homogeneity. For $CaMn_2Ox$-lactate the metal molar ratios was more variable and homogeneity significantly less (ESI† Fig. S1b).

For chelated cobalt materials the ν_{as} $-CO_2Co$ was at 1533 and ν_s at 1393 cm^{-1} (Figure 1f-g), split C-O bands were present around 1015-1100cm^{-1}. Co-OH vibrations were present at 1120cm^{-1} together with Co-OH skeletal vibrations below 1000 cm^{-1}.

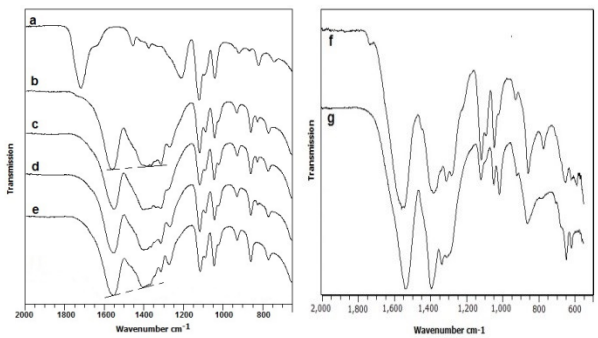

Fig. 1. FT-IR of (a) lactic acid ; (b) $CaMn_2Ox$-lactate; (c) $CaMn_3Ox$-lactate; (d) $CaMn_4Ox$-lactate; (e) Mn_3O_4-lactate; (f) Co:lactate 1:2; (g) Co-lactate 1:1. Dotted lines show increase in relative intensity of νs (CO_2^-) absorbance band at ~1400 cm^{-1} with Ca^{2+} content.

Transmission electron microscopy (TEM) of the prepared chelated samples showed that the manganese and calcium manganese materials consisted of nanoscale plate like crystals which were formed into spherules by the stirred reaction. The Mn_3O_4-lactate spherules were approximately 100nm in diameter (Fig. 2a), in comparison the Ca-Mn lactates had more prominent plate like surfaces. Ca:4Mn lactate spherules were typically 140-160nm in diameter (ESI† Fig. S2a), the Ca:3Mn lactate being slightly larger at ~170nm on average (Fig. 2b) and Ca:2Mn were smaller at around 100nm (ESI† Fig. S2b). Co-lactates however consisted of homogeneous roughly spherical nanoparticles of

measured average of 1-2nm diameter (ESI† Fig S2d) or 4.5nm (Fig. 2c) for Co:lactate 1:2 or 1:1 respectively.

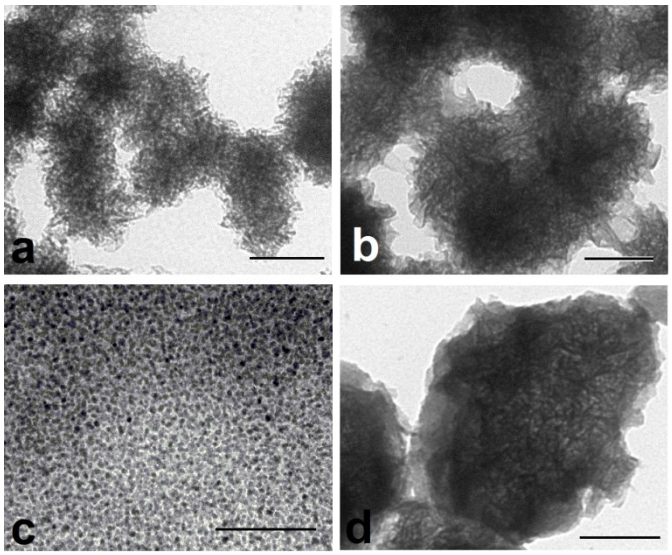

Fig. 2. TEM images showing (a) Mn_3O_4-lactate; (b) $CaMn_3Ox$-lactate; (c) Co-lactate 1:1 (average size 4.5nm); (d) $CaMn_3Ox$-lactate recovered from photocatalytic reaction after 200 min with cobalt oxide coating formed in-situ. (Scale bars = 100nm)

Dynamic light scattering was used to confirm the hydrodynamic diameter of the Co-lactates, intensities were centered around 0.8 and 4.4nm for Co:lactates 1:2 and 1:1 respectively (ESI† Fig. S2e,f).

Powder XRD measurements gave only broad reflections consistent with nanoparticulate material, Co-lactates required heating to 550°C to increase crystallinity for measurable reflections from spinel Co_3O_4 to be obtained. Mn_3O_4-lactate and a $CaMn_3Ox$-lactate sample were heated to 325°C. XRD of these treated samples showed the presence of the corresponding spinel Mn_3O_4 and CaMn oxide (ESI† Fig. S3).

XPS analysis of the washed chelated catalysts are shown in ESI† Fig. S4(a-d), this gave surface molar ratios of Ca:Mn of 1:6.8, 1:5.3, and 1:3.3 for $CaMn_4Ox$-lactate, $CaMn_3Ox$-lactate and $CaMn_2Ox$-lactate respectively due to preferential calcium leaching. High resolution XPS of the Mn 2p energy level for the samples are shown in ESI† Fig. S5. This shows a reduction in Mn peak intensity with increasing Ca presence. Also the $2p_{3/2}$ energy level situated at 640-642 eV shows a small shift to higher binding energies with the $CaMn_3Ox$-lactate indicating the presence of an elevated level of Mn^{4+}.[24, 25] XPS of the Co:lactate 1:2 sample showed the O1s band at 532 eV and $Co2p_{3/2}$ at 781.6 and $2p_{1/2}$ at 797, each with adjacent shoulders (ESI† Fig. S6), consistent with Co^{2+} bound with hydroxyls.[26]

Similarly, visible spectrometry of Co:lactate 1:2 and 1:1 samples show a single absorbance band centered at ~500nm that is associated with the Co^{2+}-O absorbance.[27] The laser ablated spinel Co_3O_4 sample gave two absorbance bands associated with both Co^{2+}-O(tet) at 420nm and Co^{3+}-O(oct) at 750nm (Fig.3).[28, 29] Overall this suggests that with chelated cobalt, samples are complexed with hydroxyl groups and the sample exists as molecular or nanoparticulate $_2$(HO)-Co-$O_2C(CH_3)COH$ at Co:lactate 1:2 and 1:1 respectively.

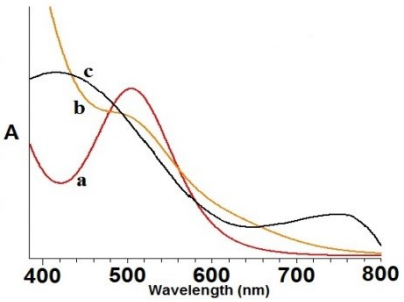

Fig. 3. Visible absorption spectrum of (a) Co-lactate 1:2; (b) Co-lactate 1:1; (c) Co_3O_4 nanoparticles.

Water oxidations

Onset of water oxidation yielding O_2 occurred within ~5 min with the catalysts with the exception of Co:lactate 1:1 sample which showed a longer lag time with onset of O_2 generation after ~10min.. A commercial laser ablated nanoparticulate Co_3O_4 resulted in O_2 yield consistent with reported values and O_2 generation occurred for approximately 1hr. For this catalyst under the conditions used the O_2 release profile points to a single effective water oxidation stage. As buffer and electron acceptor begin to be depleted, the excited state light sensitizer resorts to decomposition of its bipyridyl groups and release of CO_2 as marked by the overall downturn in measured net O_2 from ~90 min onwards (Fig. 4a). Significantly, the chelated manganese oxide based materials differed in that two distinct stages of water oxidation were obtained (Fig. 4d-g).

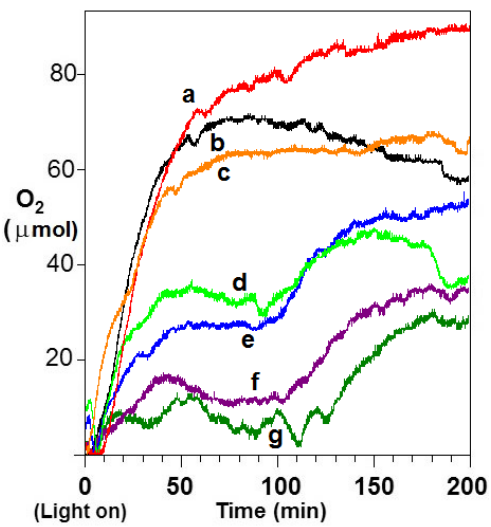

Fig. 4. Graph of O_2 release with time for water oxidation reactions using a commercial Co_3O_4 nanopowder and a range of chelated metal oxide catalysts. (a) Co:lactate 1:1; (b) commercial Co_3O_4; (c) Co:lac 1:2; (d) $CaMn_3Ox$-lactate; (e) Mn_3O_4-lactate; (f) $CaMn_4Ox$-lactate; (g) $CaMn_2Ox$-lactate.

There are several possible factors that could cause the initial and secondary O_2 generation stages separated by a cessation period. Firstly the charge on the metal oxide particle surfaces needs to re-accumulate. Since a moderate light intensity was used, time was required for build-up of charge to the reach MO^{4+} at which point water oxidation at the particle surface could resume. Secondly the $[Ru^{3+}(bipy)_3]Cl_2$ resorts to electron extraction from surrounding organics if sufficient metal oxide is not available. Some degradation of the electron acceptor and bound lactate groups (as indicated CO_2 generation and so net drop in O_2 level) together with some dissolution at the metal oxide particle surfaces occurred in this lag phase. Oxidation of $Co(OH)_x$ from decomposed electron acceptor that attached to the chelated catalysts may also be a factor. This could derive from continued electron donation for Ru^{3+} reduction but with little or no concomitant water oxidation whilst the Co_3O_4 phase was formed. Some decomposition of lactate may also contribute to decrease in O_2 levels in lag phases and also after extended reaction times around 180 min as shown in Fig. 4.

From the results it was clear that for bimetallic catalysts those prepared at a Ca:Mn ratio of 1:3 were the most efficient in terms of O_2 generation from the initial water oxidation cycle, this sample also gave the highest TOF and quantum yield (Φ) of the chelated catalysts. Mn_3O_4-lactate was intermediate followed by $CaMn_4Ox$-lactate, with $CaMn_2Ox$-lactate giving the lowest yield. With this calcium rich catalyst a relatively high TOF was obtained, but was not sustained and it is likely the low O_2 yield in the initial water oxidation stage is simply due to insufficient active Mn being present. For chelated bimetallic samples it was found that the second water oxidation yielding O_2 occurred with onset at around 90min. The amount of O_2 released was roughly inversely proportional to the magnitude of the initial cycle, and related to degree of depletion of electron acceptor and buffer.

For Co:lactates TEM observations of samples removed at intervals (not shown) suggested that gradual aggregation in the reaction mixture into clusters took place. The results suggest that oxidation of Co^{2+} to Co^{3+} by Ru^{3+} electron extraction occurs initially (without O_2 generation),[30] subsequent oxidations to the active Co^{4+} with rapid onset of water oxidation and Co^{3+}-Co^{4+} cycling then takes place.[31] The high surface area of Co-lactate 1:2 clusters led to high initial TOF. Conversely the lower surface area of Co:lactate 1:1 resulted in a lag due to the Co^{2+} to Co^{3+} conversion before sustained and effective water oxidation cycles. Lactate presence may have stabilized the $Ru(bipy)_3$ complex to some extent as net O_2 levels remained constant or rose slightly after ~100min.

Change in pH of photocatalytic reactions

Change in pH from light-on over the course of the 200min photocatalytic reaction using different catalysts was monitored (Fig. 5). During the light shielded equilibration period pH remained constant at 5.2. At light-on with Co_3O_4 nanopowder or $CaMn_3Ox$-lactate, initially change in pH was slowed due to the buffer. The results show that thereafter pH of the reaction was dominated by ammonia release from decomposed electron acceptor. As buffer became depleted the increase in pH accelerated before virtually levelling off at ~pH 8.4 after 140min. pH changes had broadly similar profiles, a difference was the commercial Co_3O_4 showed initially higher and subsequently lower pH rise reflecting the respective O_2 release profiles. However, with Co:lactate 1:2 as catalyst, measured pH rise to the levels at which sensitizer becomes unstable was rapid from the outset, which probably caused a premature reaction shutdown. pH rise was moderated with the larger sized Co:lactate 1:1 and water oxidation continued for longer with this catalyst.

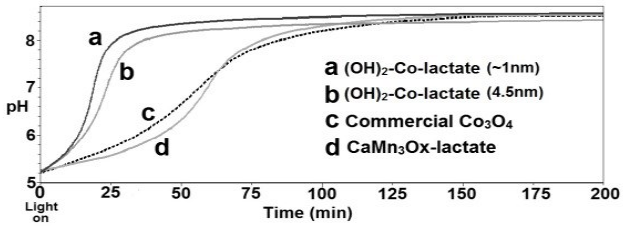

Fig. 5. Change in pH for a photocatalytic water oxidation utilizing $[Ru(bipy)_3Cl]^{2+}$, $[Co(NH_3)_5Cl]^{2+}$ (electron acceptor) and catalyst suspended in N_2 degassed aqueous acetate buffer solution at pH 5.2. Time course using Co-lactates, $CaMn_3Ox$-lactate, and commercial Co_3O_4 (with 10mg metal oxide present in all cases).

Comparison to a sintered $CaMn_3O_6$ powder was also conducted using the same experimental protocol as used with the chelated counterparts. This produced a good initial O_2 yield and TOF but no second water oxidation stage was obtained and an abrupt and marked decomposition occurred after ~30min as shown by downturn in net O_2 (Fig. 6a). The abrupt cessation rather than characteristic gradual decrease allowed particularly high Φ for the active phase with this sample. Addition by injection following equilibration, which reduced the potential for catalyst dissolution, gave improved O_2 yield, high TOF and Φ, but again no secondary water oxidation was obtained (Fig. 6b).

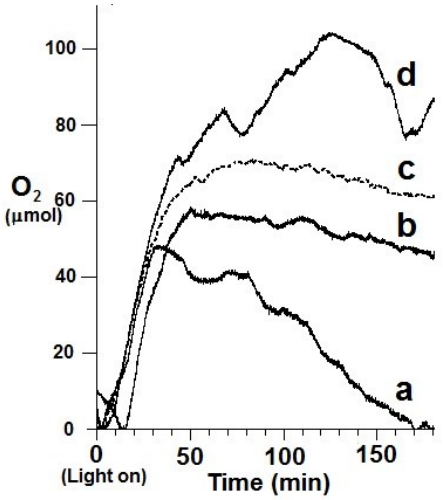

Fig. 6. Graph showing O_2 generation with $CaMn_3Ox$-lactate catalysts under different reaction protocols. (a) 10mg of $CaMn_3O_6$ stirred in reaction mixture in dark for 45 min prior to light on; (b) 10mg of $CaMn_3O_6$ added by injection to reaction flask at light on; (c) 10mg commercial nanoparticulate Co_3O_4 (for comparison); (d) 10 mg of in-situ formed Co-Mn oxide lactate recovered from previous 200min $CaMn_3Ox$-lactate photocatalytic reaction.

From these results apparent stability of this sintered material was less compared to the chelated counterpart. For reported papers no standard water oxidations conditions have yet been established and light sources, sensitizers and electron acceptors vary considerable. However, TOF's using calcium manganese oxides prepared by high temperature sintering but with matching sensitizer and sacrificial oxidant gave very comparable efficiencies.[22]

Recycling of catalyst

The O_2 yield and lifetime of a second water oxidation stage was limited due to the elevated pH at that period. Therefore in order to investigate the effect of reaction conditions on the catalyst and also its reusability, the best performing Ca:3Mn-lactate with its acquired coating was collected and reused in a new photocatalytic reaction. A rapid and two stage output was obtained with a total yield in excess of 100 µmol of O_2, which is ~85% of maximum 120µmol theoretical O_2 yield based on electron acceptor concentration (Fig. 6d). It should be noted that to obtain the high response it was necessary to inject the catalyst to the stirred reaction flask after the 45 min light shielded equilibration period.

Conversion of catalyst in-situ

It was found that at longer reaction timescales the manganese based chelated catalysts had re-organized in the stirred photocatalytic reactions as macroscopic black particles that could be easily collected by filtration. Samples from a $CaMn_3Ox$-lactate catalyzed reaction were extracted at time intervals of 50, 100, 150, 200 min washed with water and examined by TEM. This showed the presence of aggregates composed of the original nanoscale catalyst spherules which had been rounded off in shape to some extent and accumulated a coating of nanoparticulate material (Fig. 7).

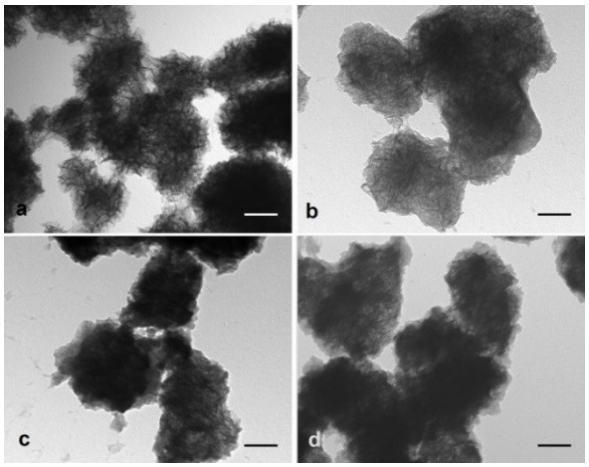

Figure 7. TEM images of $CaMn_3Ox$-lactate recovered from photocatalytic reaction after (a) 50 min; (b) 100min (c) 150 min; (d) 200 min showing accumulation of cobalt oxide coating. (Scale bar = 100nm).

Bulk EDX analysis of washed samples removed at intervals showed increase in relative levels of bound cobalt (ESI† Fig. S7). From these results, which broadly reflect pH change, cobalt accumulation was found be very gradual initially and then accelerated during the lag phase between water oxidation stages at around 100min to give a final Co:Mn mole ratio of 3.7:1 at 200 min (Fig. 8).

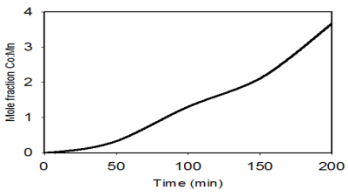

Fig. 8. Graph of increase in Co:Mn mole fraction for $CaMn_3Ox$-lactate samples recovered at intervals from photocatalytic reaction as measured by quantitative EDX analysis.

Sample	1st stage O_2 (µmol)	Max O_2 (µmol)	O_{2max}/ µmol s^{-1}	TOF_{max} $10^{-3}/s^{-1}$	ΦO_2% (at t = O_{2max})
Co_3O_4	71	(-) 71	0.0330	0.265	38.9%
Co:lactate 1:2(~1nm)	64.5	(-) 64.5	0.0434	0.350	35.3%
Co:lactate 1:1(4.5nm)	87	(-) 87	0.0382	0.305	25.6%
Mn_3O_4-lactate	28	(27)55	0.0226	0.173	12.0%
$CaMn_4Ox$-lactate	16	(17)35	0.0097	0.088	7.7%
$CaMn_3Ox$-lactate	36	(12)48	0.0316	0.386	14.0%
$CaMn_2Ox$-lactate	13	(17)30	0.0174	0.318	6.6%
Sintered $CaMn_3O_6$					
Stirred in mixture before LO	48	(-) 48	0.0400	0.403	66.0%
Added at LO	58	(-) 58	0.0486	0.487	50.8%
Re-used $CaMn_3Ox$-lactate					
Stirred in mixture before LO	43	(-) 43	0.0257	0.314	26.9%
Added at LO	85	(20) 105	0.0410	0.501	38.3%

Table 1. Table of maximum net O_2 generated and production rate and calculated TOF's. (TOF as mol O_2/ mol (active)metal s). Brackets denote contribution from a second water oxidation stage if present. (LO = light on). Quantum yield ΦO_2% = O_2 produced at t=O_{2max}/ photons absorbed at t=O_{2max} x 400% (4 photons absorbed per O_2). (Example calculations are shown in the ESI†).

XPS analysis (which gives information on the uppermost surface ~10nm) of recovered $CaMn_3Ox$-lactate catalyst from a 200min photocatalytic reaction showed the presence of cobalt and manganese at a higher mole ratio of 7.3:1. High resolution XPS analysis over the Co 2p region of samples recovered at time intervals showed onset of two bands consistent with spinel Co_3O_4 and increasing broad bands associated with hydroxide presence (Fig. 9). Similarly the O 1S region showed a O-Co band consistent with Co_3O_4 for samples taken at 50 min, at longer timescales an adjacent band due to hydroxyl build up was present (ESI† Fig. S8).[26, 32, 33] This suggests that a coating of Co from decomposed electron acceptor as near pure Co_3O_4 was formed initially. This subsequently became enriched with $Co(OH)_x$ as pH of the reaction increased and potential for oxidation of coating into Co_3O_4 reduced. Previous studies have shown that cobalt as solvated Co^{2+} ions has very little or no catalytic activity and precipitation and conversion to oxide was a prerequisite for measurable O_2 production.[34, 35] FT-IR of the recovered catalysts still showed absorption bands due to lactate binding of metal ions (ESI† Fig. S9).

O_2 yields and generation stages, TOF and quantum yields for the samples tested are shown in Table 1.

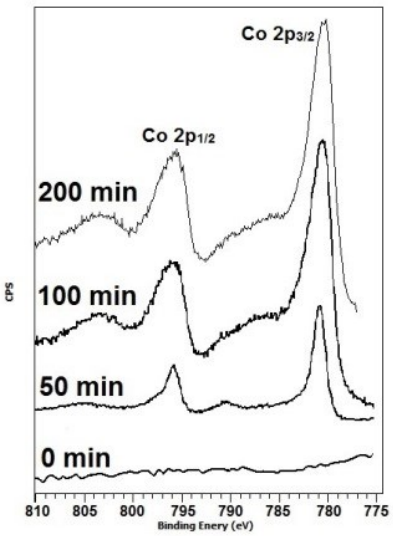

Figure 9. High resolution XPS analysis of $CaMn_3Ox$-lactate catalysed photocatalytic reaction with washed samples recovered at intervals showing accumulation of Co from decomposed electron acceptor. The Co2p region has band position and shape consistent with cobalt oxide as Co_3O_4 together with broader bands of increasing intensity indicating increasing hydroxide presence.

The suggested processes taking place in the visible light promoted water oxidation system with chelated calcium manganese oxides and hydroxylated Co-lactates are shown in Scheme 1a,b.

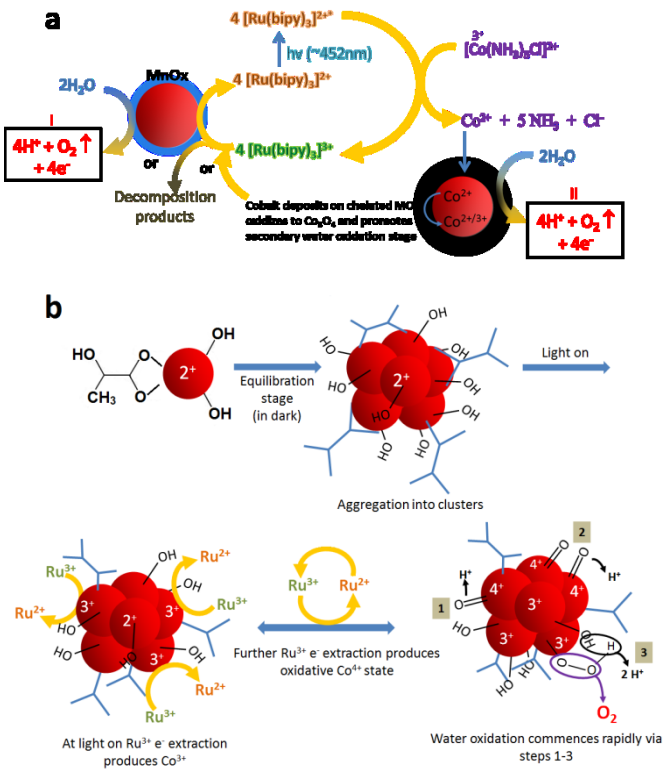

Scheme 1.(a) Photocatalytic oxidation of water by three component system showing light sensitizer, spherulitic manganese oxide based (MO) catalysed water oxidation and electron acceptor decomposition pathway. Cobalt oxide coated lactate MO catalysts are generated in-situ and promote a secondary water oxidation stage. (b) Processes leading to water oxidation for hydroxylated Co-lactates. Co^{2+} is firstly oxidized to Co^{3+} (without O_2 generation), the Co^{4+} state is then briefly formed with concomitant water oxidation cycling. (For details of cobalt oxide catalysed water oxidation processes see [31]).

TEM observation of the sintered catalysts showed that virtually no decoration of individual particles accumulated after 200 min of photocatalytic reaction (ESI† Fig. S10). Debris obtained with the sintered catalysts was inactive in re-starting further water oxidation, in contrast to the chelated manganese oxide based materials.

Conclusions

It was found that lactic acid could be used to easily prepare nanoscale chelated particles that were effective catalysts, without high temperature sintering. These were prepared in the form of solid films that were readily suspended in water which avoided possible hazardous nanopowder inhalation.

The calcium-manganese lactates represent a very simple synthetic or primitive analogue of the PSII cluster and the results suggest Ca^{2+} present at a suitable level relative to Mn played an important role in promoting water oxidation.[2, 36] Under the reaction conditions the lactate samples prepared at a Ca:3Mn molar ratio generated superior O_2 yield in the initial water oxidation relative to the other chelated bimetallic and a solely manganese catalyst. This is despite the actual Mn content being greater with the chelated Mn_3O_4 and Ca:4Mn samples. It may be that initially a proportion of the water oxidation reaction occurs via the efficient Mn^{3+}-(O^{2-})-Ca^{2+} intermediate in a manner similar to that believed to occur in the PSII $CaMn_4$ cluster. More likely is that, as indicated by XPS, an increased level of Mn with +4 character was present with this catalyst. Mn oxidation states of mixed $Mn^{3+/4+}$ have been associated with higher activity in catalysts for water oxidation and a consensus in the literature suggests an ideal averaged Mn oxidation state of +3.5-3.8 for water oxidations.[8, 37, 38] Calcium at higher level in the initial catalyst synthesis compared to the PSII cluster was required to compensate for depletion of surface Ca^{2+} in solution.

Furthermore, the chelated calcium-manganese oxides spherules could act as catalysts initially and subsequently as pre-catalyst substrates. These were able to convert in-situ to catalytically highly active nano-micro Co-Mn spinel oxide particles due to apparent preferential dissolution of Ca^{2+}, capture of waste cobalt ions from decomposed electron acceptor and its oxidative conversion into a Co_3O_4 rich nanoparticulate coating.

For Co:lactates the analysis suggests that prepared samples formed as a molecular or nanoparticulate hydroxylated complex $_2$(OH)-Co-lactate. Co^{2+} oxidations in photocatalytic reactions generated an active catalyst with high TOF and O_2 yield. Rapid pH rise with the high surface area catalyst caused premature decomposition of sensitizer. With lower surface area Co:lactate nanoparticles during photocatalysis the pH rise was more moderate and an optimal balance between respective reagents in the cyclic reaction was met.

Overall, cobalt based catalysts were superior in terms of O_2 yield and appeared more stable to reaction mixture pH. However, chelated calcium manganese oxides gave two stages of water oxidation within a single reaction run due to Co_3O_4 being formed in-situ from captured decomposed electron acceptor. These generated Co-Mn particles could be easily recycled in further reactions to give very high O_2 yields. The in-situ generation of a new catalyst was quite significant within 1 hour of photocatalytic reaction time and the results suggest that the decomposition pathway of the electron acceptor may need to be a consideration in these type of reactions. Research on improving efficiency and prolongation of the photocatalyzed reactions is currently underway.

Experimental

Reagents were obtained from Sigma-Aldrich and used as supplied. Full instrumental and data collection details are shown in the ESI†.

Preparation of chelated calcium manganese oxides

In preliminary studies calcium manganese oxide were prepared using tartaric, malic and lactic acid as potential chelating agents. All showed some degree of activity as catalysts in water oxidations, with lactate bound products giving highest O_2 yields. Therefore the calcium manganese oxide lactates were carried forward for this work. These bimetallic oxides were prepared with Ca:Mn at molar ratios of 1:2, 1:3 and 1:4. For example $CaMn_3$Oxide-lactate was prepared by dissolving 0.920g $(CH_3CO_2)_2Mn.4H_2O$ and 0.295 $Ca(NO_3)_2.4H_2O$ in 40ml of ethanol at 70°C. When the mixture began to turn light brown 0.98g of $CH_3CHCOOH$ (DL lactic acid as 85wt% solution in water) was added and the mixture stirred for a further 5 min at ~60°C before cooling to room temperature. Ammonia solution was then added dropwise with stirring to raise the pH from ~3.5 to 10.2, which was accompanied by a darkening of the solution to give a dark brown coloured liquid. The mixture was stirred for a further 10 minutes before being heated briefly in a microwave to approximately 70°C (to promote the formation of spinel oxides and binding of chelate to the nanoparticle).[39] The solution was then left in a fume hood overnight for evaporation of the ethanol and ammonia. A thick dark brown paste was formed which suspended in deionized (DI) water to give a brown coloured solution that precipitated a brown coloured floc upon standing. pH of the resulting calcium manganese oxide-lactate in water was ~5.8. The flocs responded to an applied strong magnet. TGA analysis to 800°C (not shown) of the dried powders determined that all samples consisted of 70-75wt% metal oxide. N_2 Brunauer-Emmett-Teller (BET) surface area measurements (in m^2/g) of the washed and ground samples were as follows: Mn_3O_4-lactate = 309.7(+/-2.2), $CaMn_4$Ox-lactate = 301.1(+/-1.73), $CaMn_3$Ox-lactate = 265.1(+/-1.54), $CaMn_2$Ox-lactate = 311.4(+/-1.95).

Preparation of chelated cobalt oxides

Cobalt oxide lactates were prepared by suspending 2.4g of $Co(COOCH_3)_2.4H_2O$ in 120ml of ethanol with stirring and warming to 70°C. 1.96g or 0.98g of 85% DL lactic acid was then added (giving Co:lactate of ~1:2 and 1:1) with stirring to give a purple coloured suspension. After the mixture was allowed to cool ammonia solution was added dropwise with stirring until the pH was raised from ~5.1 to 10.3 to give a clear brown/black solution. This mixture was then microwaved to ~70°C, whereupon the mixture changed colour to a deep ruby red and the resulting solution was left to cool. The solution was filtered through a 0.22µm syringe filter and the filtrate solution air dried to form a deep red solid. This was re-suspended in water and dialysed (MWCO 12-14k dialysis tubing) against DI water for 3 hours with hourly changes of water to remove salts. Purified Co:lactate 1:2 dried to form a red/black shiny solid, Co:lactate 1:1 formed shiny red/brown solids. The dried products responded to an applied strong magnet. TGA analysis to 800°C showed cobalt oxide was present at 25wt% and 27wt% with Co:lactate 1:2 and 1:1 respectively. Allowing for adsorbed water loss up 110°C , the residual wt% increases to 33% and 30% respectively. (Calculated surface area for 4.5 and ~1nm Co_3O_4 particles (by TEM/DLS) is 218 and >900 m^2/g respectively). (Products differed in appearance to cobalt lactate ($Co(O_2C(CH_3)OH)_2.H_2O$) which is a light pink crystalline powder).

Water oxidations

From TGA a consistent weight of 10 mg of inorganic component could be calculated for each chelated composite for use in the photocatalytic reaction. Nitrogen degassed DI water was used to prepare an acetate buffer of pH 5.2 (50mM sodium acetate adjusted with acetic acid). A custom made glass 50ml flask was taken and 120 mg of $[Co(NH_3)_5Cl]Cl_2$ (98%) electron acceptor and 45mg $[Ru(bipy)_3]Cl_2.6H_2O$ (99.95%) sensitizer added together with 30ml of buffer. The reaction flask was covered with foil to shield from light before either 14mg for manganese based chelates, 10mg of commercial Co_3O_4 nanopowder, 37mg (Co:lactate 1:2 (1nm)) or 34mg (Co:lactate 1:1 (4.5nm)) catalysts suspended in a further 5ml of the degassed buffer was added. The light shielded reaction flask was then left stirring for 45 minutes to allow the electron acceptor to fully dissolve and the system to equilibrate. In some particular instances catalyst suspended in 5ml of buffer was injected into the (vented) reaction flask after this equilibration period, rather than inclusion with the other reagents.

The light shield covering was then removed and the stirred flask illuminated by royal blue led (3W, 120 lumen, λmax 450-460 nm) held at a distance of 5cm from the edge of the reaction flask. This generated a measured output of average 1.3mW/cm^2 between 422-499nm (Solartech Inc. Solar Meter 9.4), at the reaction flask (with measured led light exposed surface area of 30.8cm^2). O_2 release was monitored using a calibrated Vernier O2-BTA O_2 gas sensor (of +/- 0.01-0.005% resolution) fitted into the flask aperture and reactions in air were conducted in the flask (zeroed after equilibration). Onset of O_2 release usually occurred within 5 min after light on and was monitored for 200 minutes. Micromoles of O_2 gas released into the known headspace volume was calculated from measured O_2 increase. A visible light absorption spectrum of a prepared reaction mixture with characteristic $[Ru(bipy)_3]Cl_2$ λ_{max} at 453nm is shown in Figure S10, Supporting Information. Water oxidations were also conducted using metal oxides prepared at high temperature. A commercial Co_3O_4 laser ablated nanopowder (Sigma-Aldrich 637025) with size range 8-70nm with average of 26nm and measured surface area of 38.7m^2/g (from N_2 BET) was used. Also tested was a $CaMn_3O_6$ nanopowder with surface area of 5.7m^2/g (from N_2 BET), prepared by heating of a precursor mixture to 800°C.[40]

pH of the buffered reaction mixtures increased (due to release of ammonia from the electron acceptor) from ~pH5.2 to ~8.4 at the 200 min end point. Replicate measurements were made for each sample, minor fluctuations in profiles marking onset and cessation of individual water oxidation cycles were obtained, but the overall patterns were very similar. O_2 output was consistent to within 6% for each replicate and representative profiles plotted on graphs shown. Control experiments in the absence of light or added catalyst gave no measurable O_2 output.

Acknowledgements

This work was supported by a departmental grant, Department of Chemistry, University of Bath, UK. We thank the Electron Microscopy Unit, School of Chemistry, University of Bristol, UK and the Microscopy and Analysis Suite, University of Bath, UK for assistance with TEM and EDX. We thank Dr A. Kulak, School of Chemistry, University of Leeds, UK for assistance with BET measurements. We also thank Dr A. Perriman and K. LeVay, School of Medicine, University of Bristol for assistance with DLS analysis.

Notes and references

[a] Dr D. Walsh, Prof M. Weller, Department of Chemistry, University of Bath, Claverton Down, Bath, BA2 7AY, UK.

[b] Dr N.M. Sanchez-Ballester, Prof K. Ariga, Supermolecules Group, National Institute for Materials Science, 1-1 Namiki, Tsukuba, Ibaraki, 305 0044, Japan.

[c] A. Tanaka, National Institute for Materials Science, 1-2-1 Sengen, Tsukuba, Ibaraki, 305-0047 JAPAN.

† Electronic Supplementary Information (ESI) available: Instrumentation data, image of aqueous solutions of prepared chelated catalysts, quantitative EDX analysis, TEM and DLS of lactates, XRD of Co_3O_4-lactate and Ca-Mn-lactate samples, XPS analysis of catalysts, EDX of reaction intermediates, high resolution XPS of Co_3O_4 coating, FT-IR of all chelated catalysts after reaction, TEM of commercial Co_3O_4 after reaction, visible light absorption of reaction mixture, example calculations of TOF and Quantum yield. See DOI: 10.1039/b000000x/

1. Y. Umena, K. Kawakami, J. R. Shen and N. Kamiya, *Nature*, 2011, **473**, 55-U65.
2. E. Y. Tsui, J. S. Kanady and T. Agapie, *Inorganic Chemistry*, 2013, **52**, 13833-13848.
3. D. J. Vinyard, G. M. Ananyev and G. C. Dismukes, *Annu. Rev. Biochem.*. 2013, **82**, 577-606.
4. J. Barber, *Inorganic Chemistry*, 2008, **47**, 1700-1710.
5. C. S. Mullins and V. L. Pecoraro, *Coord. Chem. Rev.*, 2008, **252**, 416-443.
6. J. S. Kanady, E. Y. Tsui, M. W. Day and T. Agapie, *Science*, 2011, **333**, 733-736.
7. I. Zaharieva, M. M. Najafpour, M. Wiechen, M. Haumann, P. Kurz and H. Dau, *Energy Environ. Sci.*, 2011, **4**, 2400-2408.
8. M. Wiechen, M. M. Najafpour, S. I. Allakhverdiev and L. Spiccia, *Energy Environ. Sci.*, 2014, **7**, 2203-2212.
9. C. Herrero, A. Quaranta, W. Leibl, A. W. Rutherford and A. Aukauloo, *Energy Environ. Sci.*, 2011, **4**, 2353-2365.
10. F. E. Osterloh and B. A. Parkinson, *MRS Bull.*, 2011, **36**, 17-22.
11. A. Harriman, J. M. Thomas and G. R. Millward, *New J. Chem.*, 1987, **11**, 757-762.
12. A. Harriman, M. C. Richoux, P. A. Christensen, S. Mosseri and P. Neta, *Journal of the Chemical Society-Faraday Transactions I*, 1987, **83**, 3001-3014.
13. L. L. Duan, Y. H. Xu, P. Zhang, M. Wang and L. C. Sun, *Inorganic Chemistry*, 2010, **49**, 209-215.
14. M. Hara, C. C. Waraksa, J. T. Lean, B. A. Lewis and T. E. Mallouk, *J. Phys. Chem. A*, 2000, **104**, 5275-5280.
15. N. D. Morris, M. Suzuki and T. E. Mallouk, *J. Phys. Chem. A*, 2004, **108**, 9115-9119.
16. F. Jiao and H. Frei, *Angew. Chem.-Int. Edit.*, 2009, **48**, 1841-1844.
17. D. Shevchenko, M. F. Anderlund, A. Thapper and S. Styring, *Energy Environ. Sci.*, 2011, **4**, 1284-1287.
18. D. Hong, J. Jung, J. Park, Y. Yamada, T. Suenobu, Y. M. Lee, W. Nam and S. Fukuzumi, *Energy Environ. Sci.*, 2012, **5**, 7606-7616.
19. C. Tommos and G. T. Babcock, *Biochimica et Biophysica Acta (BBA) - Bioenergetics*, 2000, **1458**, 199-219.
20. M. Najafpour, *Orig Life Evol Biosph*, 2011, **41**, 237-247.
21. M. M. Najafpour, B. Pashaei and S. Nayeri, *Dalton Trans.*, 2012, **41**, 4799-4805.
22. M. M. Najafpour, T. Ehrenberg, M. Wiechen and P. Kurz, *Angewandte Chemie International Edition*, 2010, **49**, 2233-2237.
23. Y. K. Chen, Y. F. Lin, Z. W. Peng and J. L. Lin, *J. Phys. Chem. C*, 2010, **114**, 17720-17727.
24. S. Kumar, V. S. Raju, S. Bera, K. Vijaynandhini and T. R. N. Kutty, *Nuclear Instruments and Methods in Physics Research Section B: Beam Interactions with Materials and Atoms*, 2005, **237**, 623-630.
25. A. Moses Ezhil Raj, S. G. Victoria, V. B. Jothy, C. Ravidhas, J. Wollschläger, M. Suendorf, M. Neumann, M. Jayachandran and C. Sanjeeviraja, *Applied Surface Science*, 2010, **256**, 2920-2926.
26. M. C. Biesinger, L. W. M. Lau, A. R. Gerson and R. S. C. Smart, *Applied Surface Science*, 2010, **257**, 887-898.
27. L. G. A. van de Water, G. L. Bezemer, J. A. Bergwerff, M. Versluijs-Helder, B. M. Weckhuysen and K. P. de Jong, *Journal of Catalysis*, 2006, **242**, 287-298.
28. D. Barreca, C. Massignan, S. Daolio, M. Fabrizio, C. Piccirillo, L. Armelao and E. Tondello, *Chemistry of Materials*, 2001, **13**, 588-593.
29. T. He, D. Chen, X. Jiao, Y. Wang and Y. Duan, *Chemistry of Materials*, 2005, **17**, 4023-4030.
30. T. Zidki, L. Zhang, V. Shafirovich and S. V. Lymar, *J. Am. Chem. Soc.*, 2012, **134**, 14275-14278.
31. M. Zhang, M. de Respinis and H. Frei, *Nat Chem*, 2014, **6**, 362-367.
32. S. C. Petitto and M. A. Langell, *Journal of Vacuum Science & Technology A*, 2004, **22**, 1690-1696.
33. W. Guo, Y. E, l. Gao, L. Fan and S. Yang, *Chemical Communications*, 2010, **46**, 1290-1292.
34. L. Sun, L. Hammarstrom, B. Akermark and S. Styring, *Chemical Society Reviews*, 2001, **30**, 36-49.
35. L. Duan, Y. Xu, P. Zhang, M. Wang and L. Sun, *Inorganic Chemistry*, 2009, **49**, 209-215.
36. Y. J. Park, J. W. Ziller and A. S. Borovik, *J. Am. Chem. Soc.*, 2011, **133**, 9258-9261.
37. R. J. Pace, L. Jin and R. Stranger, *Dalton Trans.*, 2012, **41**, 11145-11160.
38. P. W. Menezes, A. Indra, P. Littlewood, M. Schwarze, C. Göbel, R. Schomäcker and M. Driess, *ChemSusChem*, 2014, n/a-n/a.
39. Y. Y. Kim, K. Hore, S. R. Hall and D. Walsh, *Small*, 2009, **5**, 913-918.
40. Y. Y. Kim, D. Williams, F. C. Meldrum and D. Walsh, *Small*, 2013, **9**, 61-66.